Conductance fluctuations in chaotic bilayer graphene quantum dots

Rui Bao,[1] Liang Huang,[1,*] Ying-Cheng Lai,[2,3,4] and Celso Grebogi[4]

[1]*Institute of Computational Physics and Complex Systems, and Key Laboratory for Magnetism and Magnetic Materials of MOE, Lanzhou University, Lanzhou, Gansu 730000, China*

[2]*School of Electrical, Computer, and Energy Engineering, Arizona State University, Tempe, Arizona 85287, USA*

[3]*Department of Physics, Arizona State University, Tempe, Arizona 85287, USA*

[4]*Institute for Complex Systems and Mathematical Biology, King's College, University of Aberdeen, Aberdeen AB24 3UE, United Kingdom*

(Received 17 March 2015; published 27 July 2015)

Previous studies of quantum chaotic scattering established a connection between classical dynamics and quantum transport properties: Integrable or mixed classical dynamics can lead to sharp conductance fluctuations but chaos is capable of smoothing out the conductance variations. Relativistic quantum transport through single-layer graphene systems, for which the quasiparticles are massless Dirac fermions, exhibits, due to scarring, this classical-quantum correspondence, but sharp conductance fluctuations persist to a certain extent even when the classical system is fully chaotic. There is an open issue regarding the effect of finite mass on relativistic quantum transport. To address this issue, we study quantum transport in chaotic bilayer graphene quantum dots for which the quasiparticles have a finite mass. An interesting phenomenon is that, when traveling along the classical ballistic orbit, the quasiparticle tends to hop back and forth between the two layers, exhibiting a *Zitterbewegung*-like effect. We find signatures of abrupt conductance variations, indicating that the mass has little effect on relativistic quantum transport. In solid-state electronic devices based on Dirac materials, sharp conductance fluctuations are thus expected, regardless of whether the quasiparticle is massless or massive and whether there is chaos in the classical limit.

DOI: 10.1103/PhysRevE.92.012918 PACS number(s): 05.45.Mt, 72.80.Vp, 73.23.−b

I. INTRODUCTION

Quantum chaos is a field that studies the quantum manifestations of classical chaos [1]. Earlier works were mostly on nonrelativistic quantum systems described by the Schrödinger equation. Recent years have witnessed a tremendous interest in two-dimensional Dirac materials [2] such as graphene [3–9], topological insulators [10], molybdenum disulfide (MoS_2) [11,12], HITP [$Ni_3(HITP)_2$] [13], and topological Dirac semimetals [14,15], which has led to the emergence of the field of *relativistic quantum chaos* [16–23]. A fundamental issue of interest is to uncover and understand the phenomena of relativistic quantum origin that are not found in nonrelativistic quantum chaotic systems. A remarkable example is Klein tunneling, a uniquely relativistic quantum phenomenon, which has dramatic effects on conductance fluctuations in graphene quantum point contacts [24] and regularization of tunneling in chaotic Dirac fermion and graphene systems [20]. The focus of this paper is on a relativistic quantum manifestation that differs characteristically from its counterpart in the nonrelativistic quantum world: the presence of persistently sharp conductance fluctuations in chaotic graphene systems.

Conductance fluctuations are a fundamental phenomenon in open quantum systems. An important result is universal conductance fluctuations (UCFs) in mesoscopic systems [25–29]. The pioneering work of Lee and Stone [25] established theoretically that, for mesoscopic metal samples, when the inelastic diffusion length exceeds the sample dimensions, the conductance fluctuations are of the same order as the conductance quanta, which is independent of the sample size and of the degree of disorder at low temperatures, thereby exhibiting universal features. This result was consistent with both experimental studies [26] and numerical simulations [28].

Since the discovery of graphene [3–6], the anomalous transport behavior of its charge carriers has attracted a great deal of attention [7–9]. The phase coherent length of graphene at low temperatures can be as long as several hundred nanometers [30] or even micrometers [31]. It has been demonstrated experimentally that, for graphene quantum dots smaller than 100 nm, the conductance peaks become strongly nonperiodic, indicating a major contribution of the quantum confinement [32]. While it can be difficult for current technology to cut graphene precisely following a particular shape under 100 nm, the irregularities of the boundary often pushes the classical dynamics to the chaotic regime, yielding transport properties mimicking those of quantum chaotic scatterings and also Gaussian ensembles of the peaking spacing distributions [32]. Conductance fluctuations in graphene systems have been studied experimentally and analyzed using the framework of UCFs [33–35]. Rycerz *et al.* [36] found theoretically that for strong disorder, the fluctuation behaviors agree with the Altshuler-Lee-Stone prediction [25,37]. However, in the case of weak disorder, abnormally large conductance fluctuations (with magnitude several times larger than that in the strong disorder case) can occur, which can be attributed to the absence of backscattering due to the honeycomb lattice structure. Horsell *et al.* [38] subsequently found that the variance of UCFs in both monolayer and bilayer graphene flakes is strongly affected by elastic scattering, particularly intervalley scattering. Though the correlation of the fluctuations as a function of the Fermi energy is insensitive to the specific scattering mechanisms under common experimental conditions. For few-layer graphene flakes in contact with superconducting

*huangl@lzu.edu.cn

leads, conductance fluctuations can be enhanced if the applied voltage is smaller than the superconducting energy gap [39].

The seminal work of Jalabert, Baranger, and Stone [29] suggested that conductance fluctuations in the ballistic regime can be a probe of quantum chaos, establishing, as far as we know, for the first time a connection between quantum transport in solid-state devices and classical chaos. Subsequent works [40–47] revealed that UCFs are intimately related to the study of quantum chaotic scattering [48,49]. A result in nonrelativistic quantum chaotic scattering is that, for those with integrable or mixed (nonhyperbolic) classical dynamics, sharp conductance fluctuations can occur. This is because, in the corresponding classical phase space, there are Kolmogorov-Arnold-Moser (KAM) islands centered about stable periodic orbits, which quantum mechanically have little interaction between the corresponding bounded states and the electron waveguides (leads), leading to extremely sharp conductance fluctuations on energy scales of the same order of magnitude as the interaction energy [50]. The abrupt conductance changes are in fact a kind of Fano resonance [51–55]. However, if the classical dynamics are chaotic, due to ergodicity of classical orbits, the states will have strong interactions with the leads regardless of their positions. As a result, there is little probability for localized states with long lifetime to form, giving rise to smooth conductance fluctuations in the energy scale determined by the interaction strength. The distinct types of classical dynamics thus have marked fingerprints in the quantum conductance fluctuation patterns, which can be exploited to modulate the conductance fluctuations in quantum dot devices by controlling the corresponding classical dynamics [56,57]. We note that a closed system exhibiting chaos in the classical limit is capable of generating scarred states in the quantum regime, which are concentrations of the electronic states about certain classical periodic orbits [17,22,58,59]. However, when the system is open, the degree of localization of the originally scarred states is generally much weaker than that of the localized states in classically integrable or nonhyperbolic systems.

In relativistic quantum dots such as those made of monolayer graphene, a recent work [19] revealed that systems with mixed classical dynamics exhibit sharper conductance fluctuations than those with chaotic classical dynamics, which is similar to nonrelativistic quantum systems. However, even when the classical dynamics are fully chaotic, monolayer graphene quantum dots still permit the existence of highly localized states, leading to Fano-like resonances with sharp conductance fluctuations. This implies that quasiparticles in a chaotic graphene confinement can make the classically unstable orbits somewhat more "stable" in relativistic quantum systems, implying that the interplay between chaos and relativistic quantum mechanics can lead to phenomena that are not present in nonrelativistic quantum systems.

A unique feature of monolayer graphene is that the quasiparticles are massless Dirac fermions. However, an open issue concerns about the interplay between finite mass and chaos in relativistic quantum transport. In this paper, we address the generality of persistently sharp conductance fluctuations in relativistic quantum chaotic systems. We use chaotic *bilayer* graphene quantum dots (BGQD) as a prototypical class of systems. The key feature of bilayer graphene is that the quasiparticles have a finite mass. We find that persistently sharp conductance fluctuations are still present in BGQDs, indicating that a finite mass is not capable of breaking down the localized states. Another finding is that, in bilayer graphene quantum dots, electrons tend to "hop" between the two layers along the classical ballistic trajectory in each layer. Thus, the local density of states (LDS) for one layer does not form an "orbit" per se: An "orbit" emerges only when the LDS for both layers are combined. Our results indicate that in both massless and massive chaotic relativistic quantum systems, Fano-like resonances and sharp conductance fluctuations are a common feature. While in nonrelativistic quantum systems the resonances can be removed by making the system classically chaotic [56,57], the same cannot be expected in relativistic quantum systems. This may have implications in the development of relativistic quantum electronic devices.

II. MODEL OF CHAOTIC BILAYER GRAPHENE SYSTEMS

Bilayer graphene is composed of two coupled monolayers of carbon atoms, each with a hexagonal lattice structure. We use the AB stacking bilayer graphene model [60], which includes inequivalent A_1 and B_1 atoms in the top layer and A_2 and B_2 atoms in the bottom. The two graphene layers are arranged in such a way that the A_1 atoms are directly above the B_2 atoms, while B_1 or A_2 atoms are above or below the center of hexagons in the other layer. We consider the tight-binding model, which characterizes the electronic structure of graphene reasonably accurately [61], which is applicable to systems of a finite number of layers [7–9]. The tight-binding Hamiltonian for bilayer graphene is [60]

$$H = -\gamma_0 \sum_{l,\langle i,j\rangle} (a^\dagger_{l,i} b_{l,j} + \text{H.c.}) - \gamma_1 \sum_i (a^\dagger_{1,i} b_{2,i} + \text{H.c.}) - \gamma_3 \sum_{\langle i,j\rangle} (b^\dagger_{1,i} a_{2,j} + \text{H.c.}),$$

where $a^\dagger_{l,i}(b^\dagger_{l,i})$ and $a_{l,i}(b_{l,i})$ are creation and annihilation operators for sublattice A(B) at site $R_{l,i}$ in layer l (1,2), $\gamma_0 = t$ is the nearest-neighbor hopping energy in a single layer (hopping between different sublattices), γ_1 and γ_3 are energies for the hopping processes $A_1 \longleftrightarrow B_2$ and $B_1 \longleftrightarrow$ A2, respectively, which represent the interlayer coupling. The coupling parameters have the standard values [62]: $\gamma_0 =$ 2.8 eV, $\gamma_1 = 0.4$ eV, and $\gamma_3 = 0.3$ eV.

In the momentum space, the low-energy bands can be approximated as $E \approx \sqrt{\gamma_1^2/4 + v^2 p^2} - \gamma_1/2$, where γ_1, p, and v are the interlayer hopping energy, momentum, and Fermi velocity, respectively [63]. A quasiparticle in the bilayer graphene thus can be regarded effectively as a massive relativistic fermion [63], as opposed to massless particles in monolayer graphene [7–9,61].

To study the characteristics of quantum scattering dynamics in open BGQDs with different types of classical dynamics, we choose the cosine billiard [64,65] as the confinement domain of the quantum dot, which consists of two semi-infinite leads connecting to the billiard at $x = -L/2$ and $x = L/2$, respectively, and two hard walls: a flat one at $y = 0$ and a curved wall defined as $y(x) = W + (M/2)[1 - \cos(2\pi x/L)]$. Not only are the classical dynamics of this billiard system

well understood [64,65], but also its quantum scattering dynamics in the nonrelativistic regime [66] and for monolayer graphene [19] have been studied. Varying the geometric parameters W/L and M/L can generate a continuous spectrum of distinct types of classical dynamics. For example, for $W/L = 0.36$ and $M/L = 0.22$, the classical scattering dynamics is fully chaotic without any stable periodic orbits. For $W/L = 0.18$ and $M/L = 0.11$, the classical phase space is mixed (nonhyperbolic) with both KAM islands surrounding stable periodic orbits and chaotic sets [44]. For comparison, we also consider the case where the two parameters are chosen to lie between the chaotic and nonhyperbolic cases: $W/L = 0.27$ and $M/L = 0.165$.

To probe into the transport properties, we utilize the nonequilibrium Green's function method (NEGF) in the tight-binding framework to calculate the quantum transmission and the local density of states (LDS) [67]. In particular, the retarded Green's function is

$$G(E) = [EI - H - \Sigma_R(E) - \Sigma_L(E)]^{-1}, \tag{1}$$

where Σ is the retarded self-energy characterizing the effect of the lead and the subscripts R and L indicate the right and left leads, respectively. The transmission T is given by

$$T(E) = \mathrm{Tr}[\Gamma_L(E)G(E)\Gamma_R(E)G^{\dagger}(E)], \tag{2}$$

where $\Gamma_{L,R}(E)$ are the coupling matrices of the quantum dot for the left and right leads:

$$\Gamma_{L,R}(E) = i[\Sigma_{L,R}(E) - \Sigma^{\dagger}_{L,R}(E)]. \tag{3}$$

In the low-temperature limit, the conductance can be calculated using the Landauer formula [67]:

$$G \approx \frac{2e^2}{h}T(E). \tag{4}$$

The local density of states for the device can be obtained through

$$\rho = -\frac{1}{\pi}\mathrm{Im}[\mathrm{diag}(G)], \tag{5}$$

and the local current between the nearest-neighbor lattice point i and j is given by

$$J_{i\to j} = \frac{4e}{h}\mathrm{Im}\big[H_{ij}C^n_{ji}(E)\big], \tag{6}$$

where $C^n = G\Gamma_L G^{\dagger}$ is the electron correlation function and H_{ij} is an element of the Hamiltonian matrix [67]. To improve the computational efficiency, the transmission, LDS, and local current can be calculated using the recursive Green's function method.

III. RESULTS

A. Transmission fluctuations

We present results of transmission fluctuations through the BGQDs that correspond to three distinct types of classical dynamics: mixed, intermediate, and chaotic. For comparison, results from 2DEG quantum dots [nonrelativistic quantum dots (NRQD)] are also included. In our simulation, the maximum number of propagating modes is $N_{\mathrm{mode}} = 96$ for all cases for BGQDs, and $N_{\mathrm{mode}} = 48$ for 2DEG quantum dots, so their leads have comparable width. The boundaries for the BGQDs are zigzag in the horizontal direction. Figure 1 shows the transmission coefficient T of the three types of BGQDs versus the Fermi energy, together with the results from the 2DEG quantum dots with the same corresponding classical dynamics. We see that, for both BGQDs and 2DEG NRQDs, as the classical dynamics change from mixed to chaotic, the conductance fluctuations become progressively smooth. This is consistent with previous results of quantum chaotic scattering in monolayer graphene quantum dots (MGQDs) [19]. However, when comparing the BGQDs with the corresponding 2DEG NRQD cases, we see that for the same geometry (especially in the chaotic case, the bottom lines in both panels), the conductance fluctuations for the latter are nearly perfectly smooth, while for BGQDs there are still sharp conductance fluctuations. This phenomenon was also previously observed for MGQDs [19]. In general, while in nonrelativistic quantum systems classical chaos can effectively eliminate sharp conductance fluctuations through the destruction of highly localized states in the dot region, chaos does not seem to be as effective in removing the localized states in relativistic quantum dot systems. As a result, sharp conductance fluctuations in BGQDs persist. We emphasize that this does not mean that classical chaos has little or no effects on relativistic quantum transport—it is just that the effect is not as strong as in the nonrelativistic quantum case.

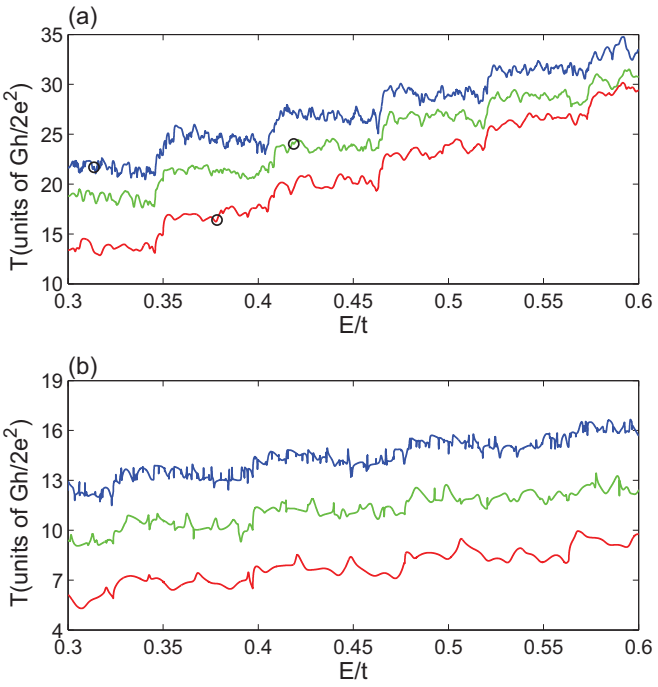

FIG. 1. (Color online) Transmission versus energy for the cosine billiard quantum dot in both relativistic and nonrelativistic regimes: (a) bilayer graphene (BGQD); (b) 2DEG quantum dot (NRQD). The blue, green, and red curves from top to bottom show the mixed, intermediate, and chaotic cases: $W/L = 0.36$ and $M/L = 0.22$, $W/L = 0.27$ and $M/L = 0.165$, and $W/L = 0.18$ and $M/L = 0.11$, respectively. The circles in (a) indicate the energy values used in Fig. 4. For all cases, we use $N_{\mathrm{mode}} = 96$ for BGQDs and $N_{\mathrm{mode}} = 48$ for 2DEG quantum dots.

In fact, from Fig. 1(a), we see that, to a certain extent, chaos does suppress the conductance fluctuations, even for massive relativistic quasiparticles in BGQDs.

B. Fano resonances and resonances width

To gain a physical understanding of the persistent sharp conductance fluctuations in BGQDs, we analyze the resonance width, the localized states, and the local current patterns. Specifically, the transmission resonance is characterized by Fano profiles [52], where the width of the resonance can be related to the localization of the electronic states [53,57,68,69], leading to sharp conductance fluctuations. In particular, the quantum transport system can be effectively regarded as an isolated quantum dot described by a Hamiltonian matrix H, which is weakly coupled to two leads, one on each side of the dot region. The eigenenergies and eigenfunctions for the isolated dot can then be calculated ($H\psi_{0\alpha} = E_{0\alpha}\psi_{0\alpha}$), yielding a set of real eigenenergies and eigenfunctions $\{E_{0\alpha}, \psi_{0\alpha} \mid \alpha = 1, \ldots, N\}$, where N is the number of discrete points (or atoms). The effect of the leads can be characterized by the retarded self-energy matrix Σ^R. The effective Hamiltonian for the dot, taking into account the leads, then can be written as $[H + \Sigma^R(E_0)]$, with a new set of eigenenergies and eigenfunctions: $\{E_\alpha, \psi_{0\alpha}\}$. Because of the coupling to the leads, electrons can "escape" from the dot region to the leads, so the eigenenergy must be complex:

$$E_\alpha = E_{0\alpha} - \Delta_\alpha - i\gamma_\alpha, \tag{7}$$

where the imaginary part is proportional to the inverse of the "lifetime" of the corresponding electron eigenstate in the dot region before entering one of the leads. The self-energy can be treated as a small perturbation to the closed dot system, because the energy has nonzero values only at the boundary points of the dot region adjacent to the leads. With respect to $E_{0\alpha}$, the new eigenenergies E_α include a shift Δ_α from $E_{0\alpha}$, and the imaginary part γ_α that characterizes the exponential decay of the wave function from the dot region. The energy scale of the resonance is determined by γ_α given by [53,57]

$$\gamma_\alpha \approx -\langle\psi_{0\alpha}|\mathrm{Im}(\Sigma^R)|\psi_{0\alpha}\rangle. \tag{8}$$

The behavior of γ_α in the complex plane of the eigenenergy provides a physical picture of the localized states and the sharp conductance fluctuations. In particular, as the Fermi energy is changed, the self-energy is a slow variable because it is mainly determined by the width of the leads. In the vicinity of the resonance energy, the self-energy can effectively be regarded as a constant. The characteristics of the resonance are mostly determined by the eigenwave function of the isolated system, $\psi_{0\alpha}$. If it is highly localized within the dot, it will have extremely small values at the boundary points where the self-energy has nonzero values, leading to a small value of γ_α and thus to a sharp resonance. On the contrary, if $\psi_{0\alpha}$ is dispersive, it typically will have large values at the boundary points, giving rise to a large value of γ_α. The effects of the wave-function patterns on the values of γ_α in BGQDs has been examined numerically.

The connection between classical dynamics and localization of the electronic states is then as follows: When the classical dynamics is integrable or mixed, there are stable

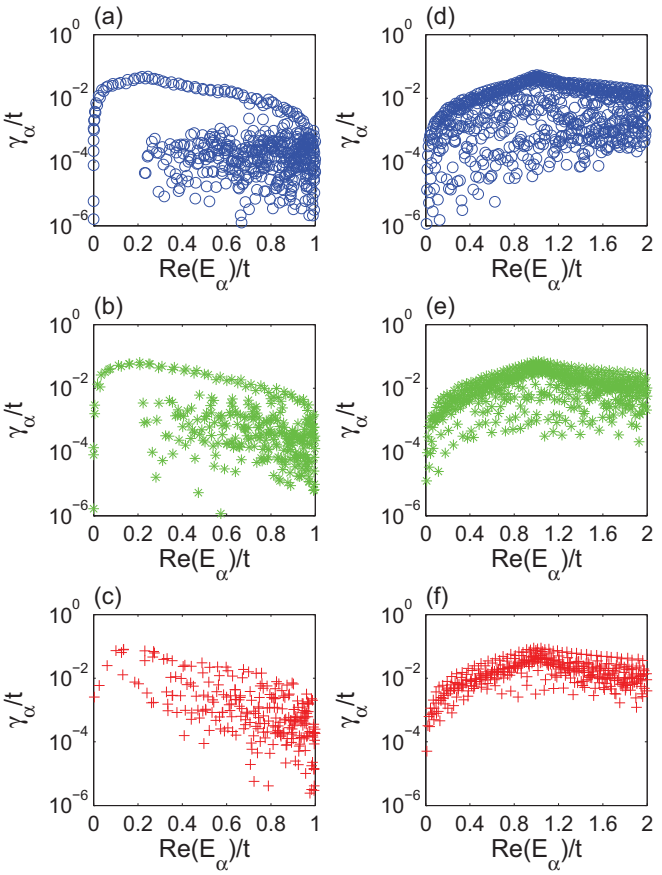

FIG. 2. (Color online) Resonance width profile γ_α for relativistic quantum dots and their nonrelativistic quantum counterparts for different types of classical dynamics: (a) BGQD, mixed (b) BGQD, intermediate (c) BGQD, chaotic, (d) NRQD, mixed, (e) NRQD, intermediate, and (f) NRQD, chaotic. The energy values at which the self-energy is evaluated are $E_0 = 0.2t$ for (a)–(c) and $E_0 = t$ for (d)–(f).

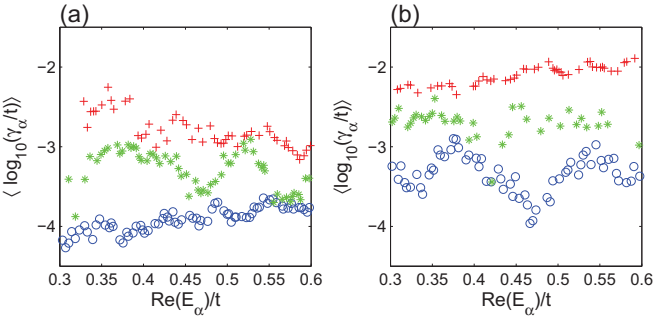

FIG. 3. (Color online) The mean value of $\log_{10}(\gamma_\alpha/t)$ in a moving window with the window size $0.04t$ and the step size $0.004t$. The upper line in different panels in Fig. 2 are excluded in the average as it accounts for the smooth variation rather than sharp conductance resonances. Panel (a) is for BGQD (left panels in Fig. 2) and panel (b) is for NRQD (right panels in Fig. 2). The blue circles, green asterisks, and red plus symbols show the mixed, intermediate, and chaotic cases, respectively.

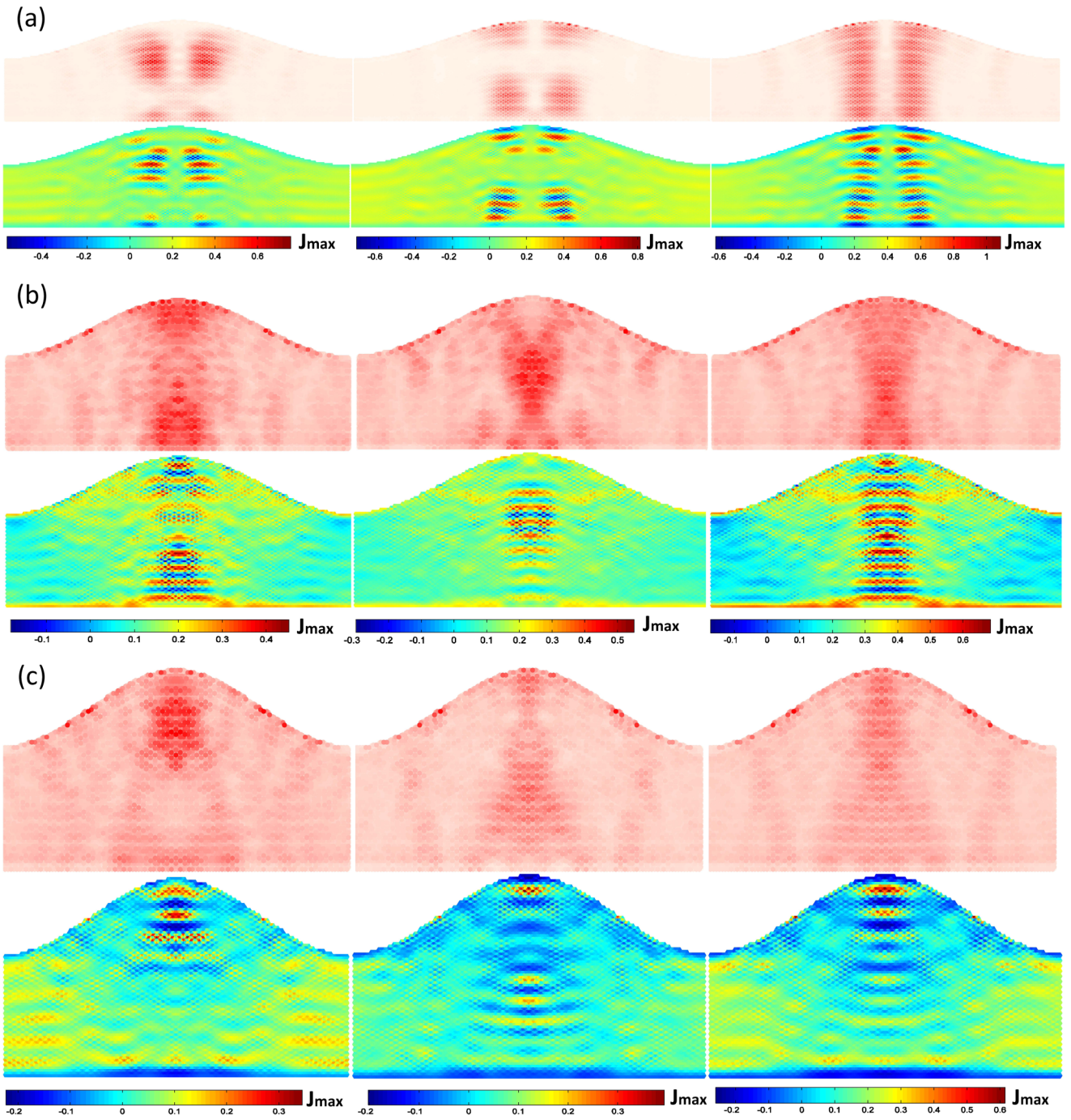

FIG. 4. (Color online) Representative local density of states (LDS, the first row) and the corresponding x component of the electron flow (the second row) for BGQDs with mixed (a), intermediate (b), and chaotic (c) classical dynamics. For the LDS patterns, the dark (red) region denotes higher values, and the color scale is normalized for each panel for better visualization. The left, middle, and right panels are for the first layer, the second layer, and combined layers, respectively. The Fermi energies are $0.3137t$ for (a), $0.4187t$ for (b), and $0.3784t$ for (c), with the respective maximum and minimum values of the LDS patterns as $(3.0016, 1.2 \times 10^{-3})$, $(0.4987, 7.7 \times 10^{-3})$, and $(0.4823, 5.6 \times 10^{-3})$.

periodic orbits about which the wave function can be strongly localized. As the classical dynamics becomes more chaotic, the KAM islands are destroyed and the periodic orbits become unstable, making it difficult to form long-lived resonant states. Thus, in general, classical chaos can smooth out conductance fluctuations. Indeed, from Fig. 1, we see that, as the classical dynamics becomes more chaotic, the conductance curve exhibit less sharp fluctuations. This reasoning suggests that γ_α for various resonant states should shift toward increasingly larger values as the classical dynamics of the system becomes progressively more chaotic.

Results from a systematic calculation of the imaginary part γ_α for the various cases are shown in Fig. 2. The energy at which the self-energy matrix is evaluated is $E_0 = 0.2t$ for

BGQD [Figs. 2(a)–2(c)] and $E_0 = t$ for NRQD [Figs. 2(d)–2(f)]. Since the calculated E_α values are accurate only in the vicinity of E_0, the energy intervals in Figs. 2(a)–2(f) are chosen to be relatively small and close to E_0. Note that the upper line of the γ_α values are in the range of $0.01t$ to $0.1t$, which correspond to the smooth variation in the conductance curve, and only the lower γ_α values correspond to the sharp conductance resonances. From Figs. 2(a) and 2(d), we see that, for mixed classical dynamics, both BGQD and NRQD have γ_α values as small as $10^{-6}t$, leading to the sharp conductance fluctuations in the top curves of Fig. 1. As the classical dynamics becomes more chaotic, the values of γ_α shift upwards, as shown in Figs. 2(b) and 2(e). For the fully chaotic case [Figs. 2(c) and 2(f)], the values of γ_α are large and their spread is small. To reveal the effect more clearly, we have plotted in Fig. 3 the averaged value of $\log_{10}(\gamma_\alpha/t)$ in a moving window to remove the fluctuations presented in Fig. 2. Since the upper line of the γ_α values correspond to the smooth variation in the conductance curve, it is excluded when doing the average.

In general, classical chaos can exert a strong effect on the conductance fluctuations for both nonrelativistic and relativistic quantum dot systems (for the latter regardless of zero or finite mass). In the relativistic quantum case, however, the effect of chaos-induced enlargement of γ is less dramatic as compared with the nonrelativistic case.

C. Localized LDS and electron flow patterns

Qualitative insights into the role of classical dynamics in the conductance fluctuation patterns in BGQDs can be gained by calculating the LDS and electron flow patterns for some representative energy values. For a bilayer graphene system, the interlayer hopping energy is relatively weak as compared to the intralayer counterpart, i.e., the values of γ_1 and γ_3 are about $1/10$ of γ_0, and the LDS and electron flow patterns are not identical for the two layers. For simplicity, we show here only the x component of the electron flow. In Fig. 4, the left and middle columns show the LDS and electron flow patterns for each layer, and the right column shows the combined patterns from both layers. We see that the LDS and electron flows are highly correlated, e.g., they are localized in the same region of the dot. The two layers are strongly coupled so the electrons flow back and forth between the two layers, as can be identified unambiguously in Fig. 4(a), where, in certain regions, the electron and its flow are mostly localized to one layer but to the corresponding adjacent regions on the other layer. When the patterns from both layers are combined, the LDS patterns reveal the underlying classical periodic orbits. The y and z components of the current show similar features. From these results, we see that the classically mixed case has relatively more pronounced localized states, but the localized patterns weaken as the classical phase space contains more chaotic regions. The degree of localization can be qualitatively described by the ratio of the maximum to the minimum values of LDS, where a larger ratio corresponds to stronger localization, as shown in Fig. 5. The typical values of the ratio for BGQDs are about 10^3, a few hundreds, and less than 100 for the mixed, intermediate, and chaotic cases, respectively. The values for 2DEG quantum dots are comparably smaller. The electron flow pattern show similar features.

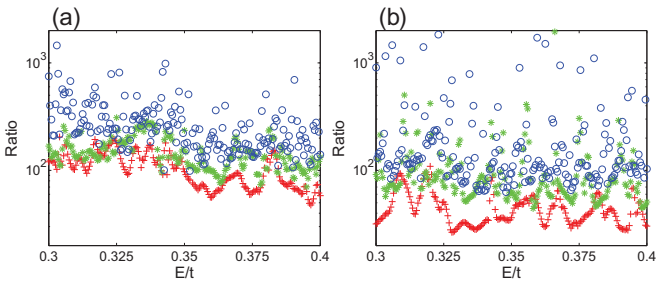

FIG. 5. (Color online) Ratio of the maximum to the minimum values of the LDS versus energy: (a) BGQD and (b) NRQD. From top to bottom the blue circles, green asterisks, and red plus symbols show the mixed, intermediate, and chaotic cases, respectively.

Through a comparison between the patterns for BGQDs and NRQDs, we see that the former exhibits more localized LDS and thus sharp conductance fluctuations. This is consistent with previous results on monolayer graphene systems in the context of transport [19], tunneling [70,71], and spectral statistics [72].

IV. CONCLUSIONS

To probe into the effect of classical chaos on relativistic quantum transport for quasiparticles with mass, we examine the transport properties of bilayer graphene quantum dots. Previous works revealed that sharp conductance fluctuations can occur in nonrelativistic quantum dot systems but only when the classical dynamics is integrable or mixed, but they persist for relativistic, massless quasiparticles (e.g., from monolayer graphene) even when the classical dynamics is chaotic. The main purpose of our work is to determine whether finite mass effect can eliminate the sharp conductance fluctuations. Our results provide a negative answer. In particular, we find that chaos has similar effect on graphene quantum dots, regardless of whether they are monolayer or bilayer. While chaos can smooth out conductance fluctuations to certain extent, its effect is weaker on relativistic quantum transport systems as compared with those on the nonrelativistic counterparts, regardless of whether the relativistic particle is massless or massive.

Transport in bilayer graphene quantum dot, however, has its own peculiar characteristics that, along a classical ballistic "orbit," the quasiparticle hops back and forth between the two layers, as evidenced by the LDS and electron flow patterns. The present work thus complements previous works to provide a more complete picture about the interplay between classical chaos and quantum transport.

ACKNOWLEDGMENTS

This work was supported by National Natural Science Foundation of China under Grants No. 11135001, No. 11375074, and No. 11422541, as well as by the Doctoral Fund of Ministry of Education of China under Grant No. 20130211110008. Y.C.L. was supported by AFOSR under Grant No. FA9550-15-1-0151.

[1] H.-J. Stöckmann, *Quantum Chaos: An Introduction* (Cambridge University Press, New York, 1999).
[2] A. H. C. Neto and K. Novoselov, Mater. Exp. **1**, 10 (2011).
[3] K. S. Novoselov, A. K. Geim, S. V. Morozov, D. Jiang, Y. Zhang, S. V. Dubonos, I. V. Grigorieva, and A. A. Firsov, Science **306**, 666 (2004).
[4] C. Berger, Z. M. Song, T. B. Li, X. B. Li, A. Y. Ogbazghi, R. Feng, Z. T. Dai, A. N. Marchenkov, E. H. Conrad, P. N. First, and W. A. de Heer, J. Phys. Chem. B **108**, 19912 (2004).
[5] K. S. Novoselov, A. K. Geim, S. V. Morozov, D. Jiang, M. I. Katsnelson, I. V. Grigorieva, S. V. Dubonos, and A. A. Firsov, Nature **438**, 197 (2005).
[6] Y. B. Zhang, Y. W. Tan, H. L. Stormer, and P. Kim, Nature **438**, 201 (2005).
[7] A. H. C. Neto, G. Guinea, N. M. R. Peres, K. S. Novoselov, and A. K. Geim, Rev. Mod. Phys. **81**, 109 (2009).
[8] N. M. R. Peres, Rev. Mod. Phys. **82**, 2673 (2010).
[9] S. D. Sarma, S. Adam, E. H. Hwang, and E. Rossi, Rev. Mod. Phy. **83**, 407 (2011).
[10] M. Z. Hasan and C. L. Kane, Rev. Mod. Phys. **82**, 3045 (2010).
[11] B. Radisavljevic, A. Radenovic, J. Brivio, V. Giacometti, and A. Kis, Nat. Nanotechnol. **6**, 147 (2011).
[12] Q. H. Wang, K. Kalantar-Zadeh, A. Kis, J. N. Coleman, and M. S. Strano, Nat. Nanotechnol. **7**, 699 (2012).
[13] D. Sheberla, L. Sun, M. A. Blood-Forsythe, S. Er, C. R. Wade, C. K. Brozek, A. Aspuru-Guzik, and M. Dincă, J. Am. Chem. Soc. **136**, 8859 (2014).
[14] Z. K. Liu, B. Zhou, Y. Zhang, Z. J. Wang, H. M. Weng, D. Prabhakaran, S.-K. Mo, Z. X. Shen, Z. Fang, X. Dai, Z. Hussain, and Y. L. Chen, Science **343**, 864 (2014).
[15] Z. K. Liu, J. Jiang, B. Zhou, Z. J. Wang, Y. Zhang, H. M. Weng, D. Prabhakaran, S.-K. Mo, H. Peng, P. Dudin, T. Kim, M. Hoesch, Z. Fang, X. Dai, Z. X. Shen, D. L. Feng, Z. Hussain, and Y. L. Chen, Nat. Mater. **13**, 677 (2014).
[16] M. V. Berry and R. J. Mondragon, Proc. R. Soc. Lond. Ser. A **412**, 53 (1987).
[17] L. Huang, Y.-C. Lai, D. K. Ferry, S. M. Goodnick, and R. Akis, Phys. Rev. Lett. **103**, 054101 (2009).
[18] L. Huang, Y.-C. Lai, and C. Grebogi, Phys. Rev. E **81**, 055203 (2010).
[19] R. Yang, L. Huang, Y.-C. Lai, and C. Grebogi, Europhys. Lett. **94**, 40004 (2011).
[20] X. Ni, L. Huang, Y.-C. Lai, and L. M. Pecora, Europhys. Lett. **98**, 50007 (2012).
[21] X. Ni, L. Huang, Y.-C. Lai, and C. Grebogi, Phys. Rev. E **86**, 016702 (2012).
[22] H. Y. Xu, L. Huang, Y.-C. Lai, and C. Grebogi, Phys. Rev. Lett. **110**, 064102 (2013).
[23] L. Ying, G.-L. Wang, L. Huang, and Y.-C. Lai, Phys. Rev. B **90**, 224301 (2014).
[24] R. Yang, L. Huang, Y.-C. Lai, and C. Grebogi, Phys. Rev. B **84**, 035426 (2011).
[25] P. A. Lee and A. D. Stone, Phys. Rev. Lett. **55**, 1622 (1985).
[26] C. P. Umbach, S. Washburn, R. B. Laibowitz, and R. A. Webb, Phys. Rev. B **30**, 4048 (1984).
[27] R. A. Webb, S. Washburn, C. P. Umbach, and R. B. Laibowitz, Phys. Rev. Lett. **54**, 2696 (1985).
[28] A. D. Stone, Phys. Rev. Lett. **54**, 2692 (1985).
[29] R. A. Jalabert, H. U. Baranger, and A. D. Stone, Phys. Rev. Lett. **65**, 2442 (1990).
[30] S. Minke, J. Bundesmann, D. Weiss, and J. Eroms, Phys. Rev. B **86**, 155403 (2012).
[31] H. Heersche, P. Jarillo-Herrero, J. Oostinga, L. Vandersypen, and A. Morpurgo, Eur. Phys. J. Spec. Top. **148**, 27 (2007).
[32] L. A. Ponomarenko, F. Schedin, M. I. Katsnelson, R. Yang, E. W. Hill, K. S. Novoselov, and A. K. Geim, Science **320**, 356 (2008).
[33] S. V. Morozov, K. S. Novoselov, M. I. Katsnelson, F. Schedin, L. A. Ponomarenko, D. Jiang, and A. K. Geim, Phys. Rev. Lett. **97**, 016801 (2006).
[34] C. Berger, Z. Song, X. Li, X. Wu, N. Brown, C. Naud, D. Mayou, T. Li, J. Hass, A. N. Marchenkov, E. H. Conrad, P. N. First, and W. A. de Heer, Science **312**, 1191 (2006).
[35] H. B. Heersche, P. Jarillo-Herrero, J. B. Oostinga, L. M. K. Vandersypen, and A. F. Morpurgo, Nature **446**, 56 (2007).
[36] A. Rycerz, J. Tworzydło, and C. Beenakker, Europhys. Lett. **79**, 57003 (2007).
[37] B. L. Al'tshuler, JETP Lett. **41**, 648 (1985).
[38] D. W. Horsell, A. K. Savchenko, F. V. Tikhonenko, K. Kechedzhi, and I. V. Lerner, Solid State Commun. **149**, 1041 (2009).
[39] D. W. Horsell, A. K. Savchenko, F. V. Tikhonenko, K. Kechedzhi, and I. V. Lerner, Nanotechnology **21**, 274005 (2010).
[40] Y.-C. Lai, R. Blümel, E. Ott, and C. Grebogi, Phys. Rev. Lett. **68**, 3491 (1992).
[41] C. M. Marcus, A. J. Rimberg, R. M. Westervelt, P. F. Hopkins, and A. C. Gossard, Phys. Rev. Lett. **69**, 506 (1992).
[42] R. Ketzmerick, Phys. Rev. B **54**, 10841 (1996).
[43] A. S. Sachrajda, R. Ketzmerick, C. Gould, Y. Feng, P. J. Kelly, A. Delage, and Z. Wasilewski, Phys. Rev. Lett. **80**, 1948 (1998).
[44] B. Huckestein, R. Ketzmerick, and C. H. Lewenkopf, Phys. Rev. Lett. **84**, 5504 (2000).
[45] G. Casati, I. Guarneri, and G. Maspero, Phys. Rev. Lett. **84**, 63 (2000).
[46] A. P. S. de Moura, Y.-C. Lai, R. Akis, J. P. Bird, and D. K. Ferry, Phys. Rev. Lett. **88**, 236804 (2002).
[47] R. Crook, C. G. Smith, A. C. Graham, I. Farrer, H. E. Beere, and D. A. Ritchie, Phys. Rev. Lett. **91**, 246803 (2003).
[48] R. Blümel and U. Smilansky, Phys. Rev. Lett. **60**, 477 (1988).
[49] R. Blümel and U. Smilansky, Physica D **36**, 111 (1989).
[50] R. Akis, D. K. Ferry, and J. P. Bird, Phys. Rev. Lett. **79**, 123 (1997).
[51] U. Fano, Phys. Rev. **124**, 1866 (1961).
[52] A. E. Miroshnichenko, S. Flach, and Y. S. Kivshar, Rev. Mod. Phys. **82**, 2257 (2010).
[53] L. Huang, Y.-C. Lai, H.-G. Luo, and C. Grebogi, AIP Adv. **5**, 017137 (2015).
[54] Y. Yoon, M.-G. Kang, T. Morimoto, M. Kida, N. Aoki, J. L. Reno, Y. Ochiai, L. Mourokh, J. Fransson, and J. P. Bird, Phys. Rev. X **2**, 021003 (2012).
[55] J. Fransson, M.-G. Kang, Y. Yoon, S. Xiao, Y. Ochiai, J. L. Reno, N. Aoki, and J. P. Bird, Nano Lett. **14**, 788 (2014).
[56] R. Yang, L. Huang, Y.-C. Lai, and L. M. Pecora, Appl. Phys. Lett. **100**, 093105 (2012).
[57] R. Yang, L. Huang, Y.-C. Lai, C. Grebogi, and L. M. Pecora, Chaos **23**, 013125 (2013).
[58] E. J. Heller, Phys. Rev. Lett. **53**, 1515 (1984).
[59] F. J. Arranz, F. Borondo, and R. M. Benito, Phys. Rev. Lett. **80**, 944 (1998).
[60] M. Koshino and T. Ando, Phys. Rev. B **73**, 245403 (2006).

[61] P. R. Wallace, Phys. Rev. **71**, 622 (1947).
[62] G. Y. Wu, N.-Y. Lue, and Y.-C. Chen, Phys. Rev. B **88**, 125422 (2013).
[63] E. McCann and M. Koshino, Rep. Prog. Phys. **76**, 056503 (2013).
[64] G. A. Luna-Acosta, K. Na, L. E. Reichl, and A. Krokhin, Phys. Rev. E **53**, 3271 (1996).
[65] G. A. Luna-Acosta, A. A. Krokhin, M. A. Rodríguez, and P. H. Hernández-Tejeda, Phys. Rev. B **54**, 11410 (1996).
[66] A. Bäcker, A. Manze, B. Huckestein, and R. Ketzmerick, Phys. Rev. E **66**, 016211 (2002).
[67] S. Datta, *Electronic Transport in Mesoscopic Systems* (Cambridge University Press, Cambridge, 1995).
[68] B. Weingartner, S. Rotter, and J. Burgdörfer, Phys. Rev. B **72**, 115342 (2005).
[69] M. Mendoza, P. A. Schulz, R. O. Vallejos, and C. H. Lewenkopf, Phys. Rev. B **77**, 155307 (2008).
[70] M.-J. Lee, T. M. Antonsen, E. Ott, and L. M. Pecora, Phys. Rev. E **86**, 056212 (2012).
[71] X. Ni, L. Huang, L. Ying, and Y.-C. Lai, Phys. Rev. B **87**, 224304 (2013).
[72] L. Huang, H.-Y. Xu, Y.-C. Lai, and C. Grebogi, Chin. Phys. B **23**, 070507 (2014).